

A 4D-Var Method with Flow-Dependent Background Covariances for the Shallow-Water Equations

BY DANIEL PAULIN^{1,2}, AJAY JASRA², ALEXANDROS BESKOS³ & DAN CRISAN⁴

¹Department of Statistics, University of Oxford, Oxford, OX1 3LB, UK.

E-Mail: *paulindani@gmail.com*

²Department of Statistics & Applied Probability, National University of Singapore, Singapore, 117546, SG.

E-Mail: *ajay.jasra@gmail.com*

³Department of Statistical Science, University College London, London, WC1E 6BT, UK.

E-Mail: *a.beskos@ucl.ac.uk*

⁴Department of Mathematics, Imperial College London, London, SW7 2AZ, UK.

E-Mail: *d.crisan@ic.ac.uk*

Abstract

The 4D-Var method for filtering partially observed nonlinear chaotic dynamical systems consists of finding the maximum a-posteriori (MAP) estimator of the initial condition of the system given observations over a time window, and propagating it forward to the current time via the model dynamics. This method forms the basis of most currently operational weather forecasting systems. In practice the optimization becomes infeasible if the time window is too long due to the non-convexity of the cost function, the effect of model errors, and the limited precision of the ODE solvers. Hence the window has to be kept sufficiently short, and the observations in the previous windows can be taken into account via a Gaussian background (prior) distribution. The choice of the background covariance matrix is an important question that has received much attention in the literature. In this paper, we define the background covariances in a principled manner, based on observations in the previous b assimilation windows, for a parameter $b \geq 1$. The method is at most b times more computationally expensive than using fixed background covariances, requires little tuning, and greatly improves the accuracy of 4D-Var. As a concrete example, we focus on the shallow-water equations. The proposed method is compared against state-of-the-art approaches in data assimilation and is shown to perform favourably on simulated data. We also illustrate our approach on data from the recent tsunami of 2011 in Fukushima, Japan.

Key words: Filtering; Smoothing; Data assimilation; Gauss-Newton Method; Shallow-Water Equations.

1 Introduction

Filtering, or data assimilation, is a field of core importance in a wide variety of real applications, such as numerical weather forecasting, climate modelling and finance; see e.g. [1, 10, 18, 36, 37] for an introduction. Informally, one is interested in carrying out inference about an unobserved signal process conditionally upon noisy observations. The type of unobserved process considered in this paper is that of a nonlinear chaotic dynamical system, with unknown initial condition. As an application in this paper we consider the case where the unobserved dynamics correspond to the discretised version of the shallow-water equations; see e.g. [58]. These latter equations are of great practical importance, generating realistic approximations of real world phenomena, useful in tsunami and flood modelling (see e.g. [6, 53]).

For systems of this type, the filtering problem is notoriously challenging. Firstly, the filter is seldom available in analytic form due to the non-linearity. Secondly, even if the given system were solvable, the associated dimension of the object to be filtered is very high (of order of 10^8 or greater) thus posing great computational challenges.

One of the most successful methods capable of handling such high dimensional datasets is the so-called 4D-Var algorithm [40, 60]: it consists of optimizing a loss-functional so that under Gaussian noise it is equivalent to finding the maximum a-posteriori (MAP) estimator of the initial condition. Since its introduction, a lot of further developments in the 4D-Var methodology have appeared in the literature; for an overview of some recent advances, we refer the reader to [3, 41, 46, 47, 48, 49]. The main focus of this article is to consider principled improvements of the 4D-Var algorithm.

It is well understood that the MAP estimator is optimal in mean square error (MSE) for linear systems (since it equals to the posterior mean for such systems, and the posterior mean is always the optimal estimator in mean square error, see page 136 of [8] for a proof). In [52], the MAP was also shown to be asymptotically optimal in MSE for a class of nonlinear systems under small observation noise or high observation frequency scenarios for a fixed observation window length. The reason for this is that in these situations, the posterior distribution near the true initial position can be well approximated by a suitably chosen Gaussian distribution, and hence the MAP estimator is close to the posterior mean, which is optimal in MSE.

Based on this theoretical result, we expect the 4D-Var method to perform well in the small-noise/high-frequency setting, when the dynamical system and the observations are

not too non-linear. In this setting, based on the results of [52], one expects the posterior distribution to be approximately Gaussian. If the conditions are not met, it is likely that the Gaussian approximation of the smoothing distribution is no longer accurate and the MAP is no longer necessarily close to optimal in MSE.

An important practical issue of the 4D-Var method is that, due to chaotic nature of the systems encountered in weather prediction, the negative log-likelihood (cost function) can become highly non-convex if the assimilation window is too long. The reason for this is that for deterministic dynamical systems, as the assimilation window grows, the smoothing distribution gets more and more concentrated on the stable manifold of the initial position, which is a complicated lower dimensional set (see [54], [51] for more details). On one hand, this means that it becomes very difficult to find the MAP estimator. On the other hand, due to the highly non-Gaussian nature of the posterior in this setting, the MAP might be far away from the posterior mean, and have a large mean square error. Moreover, for longer windows, the precision of the tangent linear model/adjoint solvers might decrease. Due to these facts, the performance of 4D-Var deteriorates for many models when the observation window becomes too long (see [34]).

The observations in the previous window are taken into account via the background (prior) distribution, which is a Gaussian whose mean is the estimate of the current position based on the previous windows, and has a certain covariance matrix. The choice of this background covariance matrix is an important and difficult problem that has attracted much research. [24] states that in operational weather forecasting systems up to 85% of the information in the smoothing distribution comes from the background (prior) distribution. The main contribution of this paper is an improvement of the 4D-Var methodology by a principled definition of this matrix in a flow-dependent way. This is based on the observations in the previous b assimilation windows (for a parameter $b \geq 1$). Via simulations on the shallow-water model, we show that our method compares favourably in precision and computational time with the state-of-the-art methods, Ensemble Kalman filter (ENKF) and En4D-Var (a 4D-Var method which uses background covariances generated by an ENKF). The main reason for the improved precision is that we do not rely on localisation, hence we can capture long range dependencies in the covariances that arise over long assimilation windows.

The structure of the paper is as follows. In the rest of this section, we briefly review the literature on 4D-Var background covariances. In Section 2 the modelling framework for

the shallow-water equations is described in detail. In Section 3 we introduce our 4D-Var method with flow-dependent background covariance. In particular, Section 1.1 compares our method with other choices of flow-dependent background covariances in the literature. In Section 4 we present some simulation results and compare the performance of our method with the ENKF and En4D-Var methods. Finally, in Section 5 we state some conclusions for this paper.

1.1 Comparison with the literature

There exist mathematically rigorous techniques to obtain the filter with precision and use the mean of the posterior distribution as the estimate, based upon sequential Monte Carlo methods (e.g. [20, 55]) which can provably work in high-dimensional systems [9]. While these approximate the posterior means and hence are optimal in mean square error, and are possibly considerably more accurate than optimization based methods, nonetheless such methodology can be practically overly expensive. As a result, one may have to resort to less accurate but more computationally efficient methodologies (see [37] for a review). There are some relatively recent applications of particle filtering methods to high dimensional data assimilation problems, see e.g. [62, 63]. While these algorithms seem to be promising for certain highly non-linear problems, their theoretical understanding is limited at the moment due to the bias they introduce via various approximations.

Despite the difficulty of solving the non-linear filtering problem exactly, due to the practical interest in weather prediction, several techniques have been devised and implemented operationally in weather forecasting centers worldwide. These techniques are based on optimization methods, hence they scale well to high dimensions and are able to process massive datasets. Although initially such methods were lacking in mathematical foundation, the books [7] and [33] are among the first to open up the field of data assimilation to mathematics. Among the earlier works devoted to the efforts of bringing together data assimilation and mathematics, we also mention [27] and [28], where a comparison between the Kalman filter (sequential-estimation) and variational methods is presented.

The performance of 4D-Var methods depends very strongly on the choice of background covariances. One of the first principled ways of choosing 4D-Var background covariances was introduced by [50]. They have proposed the so-called NMC method for choosing climatological prior error covariances based on a comparison of 24 and 48 hour forecast differences. This method was refined in [21]. [24] proposed the use of wavelets for forming background

covariances; these retain the computational advantages of spectral methods, while also allow for spatial inhomogeneity. The background covariances are made flow-dependent via a suitable modification of the NMC approach. [42] reviews some of the practical aspects of modelling 4D-Var error covariances, while [25] makes a comparison between 4D-Var for long assimilation windows and the Extended Kalman Filter. As we have noted previously, long windows are not always applicable due to the presence of model errors and the non-convexity of the likelihood.

More recently, there have been several methods proposing the use of ensembles combined with localization methods for modelling the covariances, see e.g. [66, 2, 3, 4, 5, 12, 13, 14, 15, 30, 35, 64].

Localization eliminates spurious correlations between elements of the covariance matrix that are far away from each other and hence they have little correlation. This means that these long range correlations are set to zero, which allows the sparse storage of the covariance matrix and efficient computations of the matrix-vector products. Bishop et al 2011 proposes an efficient implementation of localization by introducing some further approximations, using the product structure of the grid, and doing part of the calculations on lower resolution grid points. Such efficient implementations have allowed localized ENKF based background covariance modelling to provide the state-of-the-art performance in data assimilation, and they form the core of most operational NWP systems at the moment.

Over longer time periods, given sufficient data available, most of the variables become correlated, and imposing a localized structure over them leads to some loss of information vs the benefit of computational efficiency. Our method does not impose such a structure as it writes the precision matrix in a factorized form. Moreover, the localization structure is assumed to be fixed in time, so even with a considerable amount of tuning for a certain time period of data it is not guaranteed that the same localization structure will be optimal in the future. Our method does not make such a constant localization assumption and hence it is able to adapt to different correlation structures automatically.

We use an implicit factorised form of the Hessian and the background precision matrix described in Sections 3.2–3.3, thus we only need to store the positions of the system started from the 4D-Var estimate of the previous b windows at the observation times. This allows us to compute the effect of these matrices on a vector efficiently, without needing to store all the elements of the background precision matrix, which would require too much memory.

Although in this paper we have assumed that the model is perfect, there have been

efforts to account for model error in the literature, see [61]. The effect of nonlinearities in the dynamics and the observations can be in some cases so strong that the Gaussian approximations are no longer reasonable, see [44, 11, 26] for some examples and suggestions for overcoming these problems.

2 Notations and Model

2.1 Notations

In this paper, we will be generally using the unified notations for data assimilation introduced in [32]. In this section we briefly review the required notations for the 4D-Var data assimilation method.

The state vector at time t will be denoted by $\mathbf{x}(t)$, and it is assumed that it has dimension n . The evolution of the system from time s to time t will be governed by the equation

$$\mathbf{x}(t) = M(t, s)[\mathbf{x}(s)],$$

where $M(t, s)$ is the model evolution operator from time s to time t . In practice, this finite dimensional model is usually obtained by discretisation of the full partial differential equations governing the flow of the system.

Observations are made at times $(t_i)_{i \geq 0}$, and they are of the form

$$\mathbf{y}_i^\circ = H_i[\mathbf{x}(t_i)] + \varepsilon_i, \quad (2.1)$$

where H_i is the observation operator, and ε_i is the random noise. We will denote the dimension \mathbf{y}_i° by n_i° , and assume that $(\varepsilon_i)_{i \geq 0}$ are independent normally distributed random vectors with mean 0 and covariance matrix $(\mathbf{R}_i)_{i \geq 0}$. The Jacobian matrix (i.e. linearization) of the operator $M(t, s)$ at position $\mathbf{x}(s)$ will be denoted by $\mathbf{M}(t, s)$, and the Jacobian of H_i at $\mathbf{x}(t_i)$ will be denoted by \mathbf{H}_i . The inverse and transpose of a matrix will be denoted by $(\cdot)^{-1}$ and $(\cdot)^T$, respectively.

The 4D-Var method for assimilating the observations in the time interval $[t_0, t_{k-1}]$ consists of minimizing the cost functional

$$J[\mathbf{x}(t_0)] = \frac{1}{2}[\mathbf{x}(t_0) - \mathbf{x}^b(t_0)]^T \mathbf{B}_0^{-1}[\mathbf{x}(t_0) - \mathbf{x}^b(t_0)] + \frac{1}{2} \sum_{i=0}^{k-1} [\mathbf{y}_i - \mathbf{y}_i^\circ]^T \mathbf{R}_i^{-1}[\mathbf{y}_i - \mathbf{y}_i^\circ], \quad (2.2)$$

where $\mathbf{y}_i := H_i(\mathbf{x}(t_i))$, and \mathbf{B}_0 denotes the background covariance matrix, and $\mathbf{x}^b(t_0)$ denotes the background mean. Minimizing this functional is equivalent to maximizing the

likelihood of the smoothing distribution for $\mathbf{x}(t_0)$ given $\mathbf{y}_{0:k-1}^\circ := \{\mathbf{y}_0^\circ, \dots, \mathbf{y}_{k-1}^\circ\}$ and normally distributed prior with mean $\mathbf{x}^b(t_0)$ and covariance \mathbf{B}_0 . Note that the cost function (2.2) corresponds to the so-called *strong constraint* 4D-Var (i.e. no noise is allowed in the dynamics), there are also *weak constraint* alternatives that account for possible model errors by allowing noise in the dynamics (see e.g. [61]).

2.2 The Model

We consider the shallow-water equations, e.g. as in [58, pg. 105-106], but with added diffusion and bottom friction terms, i.e.

$$\frac{\partial u}{\partial t} = \left(-\frac{\partial u}{\partial y} + f\right)v - \frac{\partial}{\partial x} \left(\frac{1}{2}u^2 + gh\right) + \nu \nabla^2 u - c_b u; \quad (2.3)$$

$$\frac{\partial v}{\partial t} = -\left(\frac{\partial v}{\partial x} + f\right)u - \frac{\partial}{\partial y} \left(\frac{1}{2}v^2 + gh\right) + \nu \nabla^2 v - c_b v; \quad (2.4)$$

$$\frac{\partial h}{\partial t} = -\frac{\partial}{\partial x}((h + \underline{h})u) - \frac{\partial}{\partial y}((h + \underline{h})v). \quad (2.5)$$

Here, u and v are the velocity fields in the x and y directions respectively, and h the field for the height of the wave. Also, \underline{h} is the depth of the ocean, g the gravity constant, f the Coriolis parameter, c_b the bottom friction coefficient and ν the viscosity coefficient. Parameters \underline{h} , f , c_b and ν are assumed to be constant in time but in general depend on the location. The total height of the water column is the sum $\underline{h} + h$.

For square grids, under periodic boundary conditions, the equations are discretised as

$$\frac{du_{i,j}}{dt} = f_{i,j}v_{i,j} - \frac{g}{2\Delta}(h_{i+1,j} - h_{i-1,j}) \quad (2.6)$$

$$\begin{aligned} & - c_b u_{i,j} + \frac{\nu}{\Delta^2}(u_{i+1,j} + u_{i-1,j} + u_{i,j+1} + u_{i,j-1} - 4u_{i,j}) \\ & - \frac{1}{2\Delta}[(u_{i,j+1} - u_{i,j-1})v_{i,j} + (u_{i+1,j} - u_{i-1,j})u_{i,j}], \end{aligned}$$

$$\frac{dv_{i,j}}{dt} = -f_{i,j}u_{i,j} - \frac{g}{2\Delta}(h_{i,j+1} - h_{i,j-1}) \quad (2.7)$$

$$\begin{aligned} & - c_b v_{i,j} + \frac{\nu}{\Delta^2}(v_{i+1,j} + v_{i-1,j} + v_{i,j+1} + v_{i,j-1} - 4v_{i,j}) \\ & - \frac{1}{2\Delta}[(v_{i+1,j} - v_{i-1,j})u_{i,j} + (v_{i,j+1} - v_{i,j-1})v_{i,j}], \end{aligned}$$

$$\frac{dh_{i,j}}{dt} = -\frac{1}{2\Delta}(h_{i,j} + \underline{h}_{i,j})(u_{i+1,j} - u_{i-1,j} + v_{i,j+1} - v_{i,j-1}) \quad (2.8)$$

$$\begin{aligned} & - \frac{1}{2\Delta}u_{i,j}(h_{i+1,j} + \underline{h}_{i+1,j} - h_{i-1,j} - \underline{h}_{i-1,j}) \\ & - \frac{1}{2\Delta}v_{i,j}(h_{i,j+1} + \underline{h}_{i,j+1} - h_{i,j-1} - \underline{h}_{i,j-1}), \end{aligned}$$

where $1 \leq i, j \leq d$, for a typically large $d \in \mathbb{Z}_+$, with the indices understood modulo d (hence the domain is a torus), and some space-step $\Delta > 0$. Summing up (2.8) over $1 \leq i, j \leq d$,

one can see that the discretisation preserves the total mass $h_{\text{tot}} := \sum_{i,j} (h_{i,j} + \underline{h}_{i,j})$. If we assume that the viscosity and bottom friction are negligible, i.e. $\nu = c_b = 0$, then the total energy $E_{\text{tot}} := \frac{1}{2} \sum_{i,j} ((h_{i,j} + \underline{h}_{i,j})u_{i,j}^2 + (h_{i,j} + \underline{h}_{i,j})v_{i,j}^2 + g(h_{i,j}^2 - \underline{h}_{i,j}^2))$ is also preserved. When the coefficients c_b and ν are not zero, the bottom friction term always decreases the total energy (the sum of the kinetic and potential energy), while the diffusion term tends to smooth the velocity profile. We denote the solution of equations (2.6)-(2.8) at time $t \geq 0$ as

$$\mathbf{x}(t) := \left((u_{i,j}(t))_{1 \leq i,j \leq d}, (v_{i,j}(t))_{1 \leq i,j \leq d}, (h_{i,j}(t))_{1 \leq i,j \leq d} \right).$$

The unknown and random initial condition is denoted by $\mathbf{x}(0)$. One can show by standard methods (see [45]) that the solution of (2.6)-(2.8) exists up to some time $T_{\text{sol}}(\mathbf{x}(0)) > 0$. In order to represent the components of $\mathbf{x}(t)$, we introduce a vector index notation. The set $\mathcal{I} := \{u, v, h\} \times \{1, \dots, d\} \times \{1, \dots, d\}$ denotes the possible indices, with the first component referring to one of u, v, h , the second component to coordinate i , and the third to j . A vector index in \mathcal{I} will usually be denoted as \mathbf{m} or \mathbf{n} , e.g. if $\mathbf{m} = (u, 1, 2)$, then $\mathbf{x}_{\mathbf{m}}(t) := u_{1,2}(t)$.

We assume that the $n := 3d^2$ dimensional system is observed at time points $(t_l)_{l \geq 0}$, with observations described as in Section 2.1. The aim of smoothing and filtering is to approximately reconstruct $\mathbf{x}(t_0)$ and $\mathbf{x}(t_k)$ based on observations $\mathbf{y}_{0:k-1}^\circ$. We note that data assimilation for the shallow-water equations have been widely studied in the literature, see [7], [22] for the linearised form and [16], [28], [43] for the full non-linear form of the equations.

3 4D-Var with Flow-Dependent Covariance

3.1 Method Overview

Assume that observations $\mathbf{y}_{0:k-1}^\circ$ are made at time points $t_l = t_0 + lh$ for $l = 0, \dots, k-1$, and let $T := kh$. The 4D-Var method for assimilating the observations in the time interval $[t_0, t_{k-1}]$ consists of minimizing the cost functional (2.2). Under the independent Gaussian observation error assumption, $-J[\mathbf{x}(t_0)]$ is the log-likelihood of the smoothing distribution, ignoring the normalising constant. The minimizer of J is the MAP estimator, and is denoted by $\hat{\mathbf{x}}_0$ (if multiple such minimizers exist, then we choose any of them). A careful choice of the background distribution is essential, especially in the case when the total number of observations in the assimilation window is smaller than the dimension of the dynamical system, where without the prior distribution, the likelihood would be singular (see [19] for a principled method of choosing priors).

In [52], it is shown that the MAP estimator for the smoother has some desirable theoretical properties. In particular, in the small-noise/high-frequency scenario (with T fixed, $\mathbf{R}_i = O(\sigma^2)$, and $\sigma\sqrt{h} \rightarrow 0$), under some conditions, MAP is asymptotically optimal in mean-square error. In the case of the filter, similar results were shown for the push-forward map of $\hat{\mathbf{x}}_0$ to time t_k under the ODE dynamics, denoted by $M(t_k, t_0)[\hat{\mathbf{x}}_0]$. Moreover, it was shown that the smoothing and filtering distributions are approximately Gaussian when $\sigma\sqrt{h}$ is small.

To obtain the MAP estimator, we make use of Newton's method. Starting from some appropriate initial position $\mathbf{x}_0 \in \mathbb{R}^n$, the method proceeds via the iterations

$$\mathbf{x}_{l+1} = \mathbf{x}_l - \left(\frac{\partial^2 J}{\partial \mathbf{x}_l^2} \right)^{-1} \frac{\partial J}{\partial \mathbf{x}_l}, \quad l \geq 0, \quad (3.1)$$

where $\frac{\partial J}{\partial \mathbf{x}_l}$ and $\frac{\partial^2 J}{\partial \mathbf{x}_l^2}$ denote the gradient and Hessian of J at \mathbf{x}_l , respectively. Due to the high dimensionality of the systems in weather forecasting, typically iterative methods such as the preconditioned conjugate gradient (PCG) are used for evaluating (3.1). The iterations are continued until the step size $\|\mathbf{x}_{l+1} - \mathbf{x}_l\|$ falls below a threshold $\delta_{\min} > 0$. The final position is denoted by $\hat{\mathbf{x}}_*$, and this is the numerical estimate for $\hat{\mathbf{x}}_0$ - with its push-forward $M(t_k, t_0)[\hat{\mathbf{x}}_*]$ then being the numerical estimate for $M(t_k, t_0)[\hat{\mathbf{x}}_0]$. [52] shows that if the initial position \mathbf{x}_0 is sufficiently close to the true signal $\mathbf{x}(t_0)$, then Newton's method converges rapidly to MAP (in practice, a few steps suffice).

To apply the iterations (3.1), one needs to compute the gradient and the Hessian of J (or, more precisely, the application of the latter to a vector, which is all that is required for iterative methods such as PCG). An efficient method for doing this is given in the next section. In practice, one cannot apply the above optimization procedure for arbitrarily large k due to the non-convexity of the smoothing distribution for big enough k (due of the nonlinearity of the system). Therefore, we need to partition the observations into blocks of size k for some reasonably small k , and apply the procedure on them separately. The observations in the previous blocks can be taken into account by appropriately updating the prior distribution. The details of this procedure are explained in Section 3.3. Finally, in Section 1.1 we compare our method with other choices of flow-dependent background covariances in the literature.

3.2 Gradient and Hessian Calculation

We can rewrite the gradient and Hessian of the cost function J at a point $\mathbf{x}(t_0) \in \mathbb{R}^n$ as

$$\frac{\partial J}{\partial \mathbf{x}(t_0)} = \mathbf{B}_0^{-1}[\mathbf{x}(t_0) - \mathbf{x}^b(t_0)] - \sum_{l=0}^{k-1} \mathbf{M}(t_l, t_0)^T \mathbf{H}_l^T \mathbf{R}_l^{-1} (\mathbf{y}_l - \mathbf{y}_l^\circ), \quad (3.2)$$

$$\begin{aligned} \frac{\partial^2 J}{\partial \mathbf{x}(t_0)^2} &= \mathbf{B}_0^{-1} + \sum_{l=0}^{k-1} \mathbf{M}(t_l, t_0)^T \mathbf{H}_l^T \mathbf{R}_l^{-1} \mathbf{H}_l \mathbf{M}(t_l, t_0) \\ &\quad - \sum_{l=0}^{k-1} \left(\frac{\partial \mathbf{M}(t_l, t_0)}{\partial \mathbf{x}_0^2} \right)^T \mathbf{H}_l^T \mathbf{R}_l^{-1} (\mathbf{y}_l - \mathbf{y}_l^\circ) - \sum_{l=0}^{k-1} (\mathbf{M}(t_l, t_0)^T)^2 \left(\frac{\partial^2 H_l}{\partial \mathbf{x}(t_l)^2} \right)^T \mathbf{R}_l^{-1} (\mathbf{y}_l - \mathbf{y}_l^\circ). \end{aligned} \quad (3.3)$$

Let $\mathbf{M}_i := \mathbf{M}(t_i, t_{i-1})$, then $\mathbf{M}(t_l, t_0) = \mathbf{M}_l \cdots \mathbf{M}_1$, so the sum in the gradient (3.2) can be rewritten as

$$\sum_{l=0}^{k-1} \mathbf{M}(t_l, t_0)^T \mathbf{H}_l^T \mathbf{R}_l^{-1} (\mathbf{y}_l - \mathbf{y}_l^\circ) = \sum_{l=0}^{k-1} \mathbf{M}_1^T \cdots \mathbf{M}_l^T \mathbf{H}_l^T \mathbf{R}_l^{-1} (\mathbf{y}_l - \mathbf{y}_l^\circ) \quad (3.4)$$

The above summation can be efficiently performed as follows. We consider the sequence of vectors

$$\begin{aligned} \mathbf{g}_{k-1} &:= \mathbf{H}_{k-1}^T \mathbf{R}_{k-1}^{-1} (\mathbf{y}_{k-1} - \mathbf{y}_{k-1}^\circ); \\ \mathbf{g}_l &:= \mathbf{H}_l^T \mathbf{R}_l^{-1} (\mathbf{y}_l - \mathbf{y}_l^\circ) + \mathbf{M}_{l+1}^T \mathbf{g}_{l+1}, \quad k-1 > l \geq 0. \end{aligned}$$

The sum on the right side of (3.4) then equals \mathbf{g}_0 . We note that this method of computing the gradients forms the basis of the *adjoint* method, introduced in [60], see also [59].

In the case of the Hessian, in (3.3) there are also second order Jacobian terms. If $\mathbf{x}(t_0)$ is close to the true initial position, then $(\mathbf{y}_l - \mathbf{y}_l^\circ) \approx \varepsilon_l$. Therefore in the low-noise/high-frequency regime, given a sufficiently precise initial estimator, these second order terms can be neglected. Using such Hessian corresponds to the so-called Gauss–Newton method, which has been studied in the context of 4D-Var in [29]. Thus, we use the approximation

$$\widehat{\frac{\partial^2 J}{\partial \mathbf{x}(t_0)^2}} := \mathbf{B}_0^{-1} + \sum_{l=0}^{k-1} \mathbf{M}(t_l, t_0)^T \mathbf{H}_l^T \mathbf{R}_l^{-1} \mathbf{H}_l \mathbf{M}(t_l, t_0) \quad (3.5)$$

A practical advantage of removing the second order terms is that if the Hessian of the log-likelihood of the prior, \mathbf{B}_0 is positive definite, then the resulting sum is positive definite, so the direction of $-\left(\widehat{\frac{\partial^2 J}{\partial \mathbf{x}(t_0)^2}}\right)^{-1} \cdot \frac{\partial J}{\partial \mathbf{x}(t_0)}$ is always a direction of descent (which is not always true if the second order terms are included). Note that via the so-called second-order adjoint equations, it is possible to avoid this approximation, and compute the action of the Hessian $\frac{\partial^2 J}{\partial \mathbf{x}(t_0)^2}$ on a vector in $O(n)$ time, see [39]. However this can be slightly

more computationally expensive, and in the simulations in this paper the Gauss-Newton approximation (3.5) worked well.

For the first order terms in the Hessian, for any $\mathbf{w} \in \mathbb{R}^n$, we have

$$\begin{aligned} \sum_{l=0}^{k-1} \mathbf{M}(t_l, t_0)^T \mathbf{H}_l^T \mathbf{R}_l^{-1} \mathbf{H}_l \mathbf{M}(t_l, t_0) \mathbf{w} \\ = \sum_{l=0}^{k-1} \mathbf{M}_1^T \mathbf{M}_2^T \dots \mathbf{M}_l^T \mathbf{H}_l^T \mathbf{R}_l^{-1} \mathbf{H}_l \mathbf{M}_l \mathbf{M}_{l-1} \dots \mathbf{M}_1 \mathbf{w}. \end{aligned} \quad (3.6)$$

We define

$$\mathbf{w}_l := \mathbf{M}_l \dots \mathbf{M}_1 \mathbf{w}, \quad l = 0, \dots, k-1;$$

and consider the sequence of vectors

$$\begin{aligned} \mathbf{h}_{k-1} &= \mathbf{H}_{k-1}^T \mathbf{R}_{k-1}^{-1} \mathbf{H}_{k-1} \mathbf{w}_{k-1}; \\ \mathbf{h}_l &= \mathbf{H}_l^T \mathbf{R}_l^{-1} \mathbf{H}_l \mathbf{w}_l + \mathbf{M}_{l+1}^T \mathbf{h}_{l+1}, \quad k-1 > l \geq 0. \end{aligned} \quad (3.7)$$

Then the sum on the right side of (3.6) equals \mathbf{h}_0 . The Hessian plays an important role in practical implementations of the 4D-Var method, and several methods have been proposed for its calculation (see [17, 39, 38]). Due to computational considerations, usually some approximations such as lower resolution models are used when computing Hessian-vector products for Krylov subspace iterative solvers in practice (this is the so-called incremental 4D-Var method, see [17]). Note that it is also possible to use inner and outer loops, where in the inner loops both the Hessian-vector products and the gradient are run on lower resolution models, while in the outer loops we use the high resolution model for the gradient, and lower resolution model for the Hessian-vector products. [38] has studied the theoretical properties of this approximation. In practice, the speedup from this method can be substantial, but this approximation can introduce some instability, hence appropriate tuning is needed to ensure good performance.

At the end of Section 3.3, we discuss how can the incremental 4D-Var strategy be combined with the flow-dependent background covariances proposed in this paper.

3.3 4D-Var Filtering with Flow-Dependent Covariance

In this section we describe a 4D-Var based filtering procedure that can be implemented in an online fashion, with observations $\{\mathbf{y}_l^\circ\}_l$ obtained at times $t_l = lh$, $l = 0, 1, \dots$ (although the method can be also easily adapted to the case when the time between the observations varies). We first fix an assimilation window length $T = kh$, for some $k \in \mathbb{Z}_+$, giving rise to consecutive windows $[0, t_k]$, $[t_k, t_{2k}]$, \dots

Let the background distribution on $\mathbf{x}(t_0)$ be Gaussian with mean $\mathbf{x}^b(t_0)$ and covariance matrix \mathbf{B}_0 . In general, let the background distributions for the position of the signal at the beginning of each assimilation window, $\{\mathbf{x}(t_{mk})\}_{m \geq 0}$, have means $\{\mathbf{x}^b(t_{mk})\}_{m \geq 0}$ and covariance matrices $\{\mathbf{B}_{mk}\}_{m \geq 0}$. There are several ways to define these quantities sequentially, as we shall explain later on in this section. Assuming that these are determined with some approach, working on the window $[t_{mk}, t_{(m+1)k}]$ we set our estimator $\hat{\mathbf{x}}(t_{mk})$ of $\mathbf{x}(t_{mk})$ as the MAP of the posterior of $\mathbf{x}(t_{mk})$ given background with mean $\mathbf{x}^b(t_{mk})$ and covariance \mathbf{B}_{mk} , and data $\mathbf{y}_{mk:(m+1)k-1}^\circ$; we also obtain estimates for subsequent times in the window, via push-forward, i.e. $\hat{\mathbf{x}}(t_l) := M(t_l, t_{mk})[\hat{\mathbf{x}}(t_{mk})]$, $mk \leq l < (m+1)k$. Recall that the numerical value of MAP is obtained by the Gauss–Newton method (see (3.1), with the details given in Section 3.1).

We now discuss choices for the specification of the background distributions. A first option is to set these distributions identical to the first one, and set $\mathbf{B}_{mk} := \mathbf{B}_0$ and $\mathbf{x}(t_{mk}) := \mathbf{x}(t_0)$ (i.e. no connection with earlier observations). A second choice (used in the first practical implementations of the 4D-Var method) is to set $\mathbf{B}_{mk} := \mathbf{B}_0$ (the covariance is kept constant) but change the background mean to

$$\mathbf{x}^b(t_{mk}) := M(t_{mk}, t_{(m-1)k})[\hat{\mathbf{x}}(t_{m(k-1)})], \quad (3.8)$$

i.e. adjusting the prior mean to earlier observations. Finally, one can attempt to update both the mean and the covariance matrix of the background (prior) distribution, and this is the approach we follow here.

Note that we still define the background means according to (3.8). To obtain data-informed background covariances \mathbf{B}_{mk} we use Gaussian approximations for a number, say $b \geq 1$, of earlier windows of length T , and appropriately push-forward these to reach the instance of current interest t_{mk} . There are two reasons why we use a fixed b and do not push-forward all the way from time t_0 . The first is to avoid quadratic costs in time. The total computational cost for our approach up to time mT scales linearly with time for a fixed b , but if we would start from t_0 , then we would incur $O(m^2)$ computational cost (or if it is done by storing the whole covariance matrix directly, then the approach would have $O(d^2)$ memory cost which is prohibitive in practice). The second reason is that a Gaussian distribution propagated through non-linear dynamics for longer and longer intervals of length bT becomes highly non-Gaussian for large values of b , so the resulting background distribution can lead to poorer results than using smaller values of b . Reminiscent to 4D-Var, at time $t_{(m-b)k}$ we always start off the procedure with the same background covariance \mathbf{B}_0 . In [52] it was shown

– under certain assumptions – that for a class of non-linear dynamical systems, for a fixed observation window T , if $\|\mathbf{R}_i\| = O(\sigma^2)$ and $\sigma\sqrt{h}$ is sufficiently small (h is the observation time step) then the smoothing and filtering distributions can indeed be well approximated by Gaussian laws. Following the ideas behind (3.5), an approximation of the Hessian of J , evaluated at the MAP given data $\mathbf{y}_{(m-1)k:m k-1}^\circ$ is given as

$$\mathbf{B}_{(m-1)k}^{-1} + \mathbf{D}_{(m-1)k:m k-1},$$

where we have defined

$$\begin{aligned} \mathbf{D}_{(m-1)k:m k-1} &:= \sum_{l=0}^{k-1} \mathbf{A}_{m-1,l}^T \mathbf{R}_{(m-1)k+l}^{-1} \mathbf{A}_{m-1,l}; \\ \mathbf{A}_{m-1,l} &:= \mathbf{H}_{(m-1)k+l} \mathbf{M}(t_{(m-1)k+l}, t_{(m-1)k}) [\hat{\mathbf{x}}(t_{(m-1)k})]. \end{aligned}$$

If the precision (inverse covariance) of the background were 0, then $\mathbf{D}_{(m-1)k:m k-1}$ would correspond to the Hessian of J at the MAP, and the smoothing distribution could be approximated by a normal distribution with mean $\hat{\mathbf{x}}(t_{(m-1)k})$ and precision matrix $\mathbf{D}_{(m-1)k:m k-1}$. Recall the change of variables formula: if $\mathbf{Z} \sim N(m, \mathbf{P}^{-1})$ in \mathbb{R}^n and $\varphi : \mathbb{R}^n \rightarrow \mathbb{R}^n$ is a continuously differentiable function, then $\varphi(\mathbf{Z})$ follows approximately

$$N\left(\varphi(m), \left[\left(\left(\frac{\partial \varphi}{\partial m} \right)^{-1} \right)^T \cdot \mathbf{P} \cdot \left(\frac{\partial \varphi}{\partial m} \right)^{-1} \right]^{-1}\right). \quad (3.9)$$

The quality of this approximation depends on the size of the variance of \mathbf{Z} , and the degree of non-linearity of φ . A way to consider the effect of the observations in the previous b assimilation windows is therefore by using the recursion

$$\begin{aligned} \mathbf{B}_{(m-b)k}^m &= \mathbf{B}_0; \\ \mathbf{B}_{(m-b+j)k}^m &= \left[\left(\mathbf{M}(t_{(m-b+j)k}, t_{(m-b+j-1)k}) [\hat{\mathbf{x}}(t_{(m-b+j-1)k})]^T \right)^{-1} \cdot \left(\mathbf{B}_{(m-b+j-1)k}^m \right)^{-1} \right. \\ &\quad \left. + \mathbf{D}_{(m-b+j-1)k:(m-b+j)k-1} \right] \cdot \left(\mathbf{M}(t_{(m-b+j)k}, t_{(m-b+j-1)k}) [\hat{\mathbf{x}}(t_{(m-b+j-1)k})]^T \right)^{-1}, \end{aligned} \quad (3.10)$$

for $j = 1, \dots, b$, and set $\mathbf{B}_{mk} := \mathbf{B}_{mk}^m$, where we have defined

$$\begin{aligned} \mathbf{D}_{(m-b+j-1)k:(m-b+j)k-1} &:= \sum_{l=0}^{k-1} \mathbf{A}_{m-b+j-1,l}^T \mathbf{R}_{(m-b+j)k+l}^{-1} \mathbf{A}_{m-b+j-1,l}, \quad j = 1, \dots, b; \\ \mathbf{A}_{m-b+j-1,l} &:= \mathbf{H}_{(m-b+j-1)k+l} \mathbf{M}(t_{(m-b+j-1)k+l}, t_{(m-b+j-1)k}) [\hat{\mathbf{x}}(t_{(m-b+j-1)k})]. \end{aligned}$$

Note that similarly to the idea of variance inflation for the Kalman filter, one could include a multiplication by an inflation factor $(1 + \alpha)$ for some $\alpha > 0$ in the definition of $\mathbf{B}_{(m-b)k}^m$

in (3.10). To simplify the expressions (3.10), we define

$$\mathbf{M}_{-j} := \mathbf{M}(t_{(m-j+1)k}, t_{(m-j)k})[\hat{\mathbf{x}}(t_{(m-j)k})], \quad j = 1, 2, \dots, b. \quad (3.11)$$

The action of \mathbf{B}_{mk}^{-1} on a vector $\mathbf{w} \in \mathbb{R}^n$ can be computed efficiently as follows. Let

$$\mathbf{w}_{-j} := \mathbf{M}_{-j}^{-1} \cdots \mathbf{M}_{-1}^{-1} \mathbf{w}, \quad j = 1, 2, \dots, b. \quad (3.12)$$

We then determine the recursion

$$\begin{aligned} \mathcal{B}_{-b} &:= (\mathbf{M}_{-b}^T)^{-1} (\mathbf{B}_0^{-1} + \mathbf{D}_{(m-b)k:(m-b+1)k-1}) \mathbf{w}_{-b} \\ \mathcal{B}_{-j} &:= (\mathbf{M}_{-j}^T)^{-1} (\mathcal{B}_{-j+1} + \mathbf{D}_{(m-j)k:(m-j+1)k-1} \mathbf{w}_{-j}), \quad j = b-1, \dots, 1. \end{aligned} \quad (3.13)$$

Then it is easy to see that $\mathbf{B}_{mk}^{-1} \mathbf{w} = \mathcal{B}_{-1}$.

In order to evaluate the quantities in (3.12) and (3.13) for the shallow-water equations (2.6)-(2.8), we need implement the effect of the Jacobians $\mathbf{M}_1, \dots, \mathbf{M}_k$, their inverses $\mathbf{M}_1^{-1}, \dots, \mathbf{M}_k^{-1}$, and their respective transpose for the previous b assimilation windows. Note that multiplying by $\mathbf{D}_{(m-l)k:(m-l+1)k-1}$ is equivalent to evaluating (3.7) for the appropriate Jacobians, hence it is also based on multiplication by these Jacobians, their inverses and their transposes.

Matrix-vector products of the form $\mathbf{M}_j \mathbf{v}$ and $\mathbf{M}_j' \mathbf{v}$ can be computed by the tangent linear model, and by the adjoint equations, respectively. When computing matrix-vector products of the form $\mathbf{M}_j^{-1} \mathbf{v}$, and $(\mathbf{M}_j^{-1})' \mathbf{v}$, we need to run the tangent linear model backward in time, while the adjoint equations forward in time. It is important to note that while normally this would lead to numerical instability if done for a long time period (as the shallow-water equations are dissipative), this is not a problem here as we only run them over short time periods, the time between two observations (even shorter time periods could be possible if needed by breaking the Jacobians into products of Jacobians over shorter intervals). The initial point of these backward runs of the original equation (and forward runs of the adjoint equation) is always based on a forward run of the original equation, hence the instability is avoided. For the shallow-water equations, the Jacobians \mathbf{M}_j can be stored directly in a sparse format, see the Appendix for more details (this reduces the need to use the ODE solvers repeatedly during the optimization steps, however, this is not necessary for the method to work as we can always use the adjoint/tangent linear solvers directly as described above).

Since we use the forward and adjoint equations of the model, computational cost of using these b previous intervals in the calculation of the gradient and the product of the Hessian

with a vector is a Newton’s step is at most $O(b)$ times more than just using the observations in the current window. The key idea behind the choice of the precision matrices (3.10) is that we approximate the likelihood terms corresponding to the observations in the previous windows by Gaussian distributions, and then propagate them forward to the current time position via the Jacobians of the dynamics according to the change of variables formula (3.9). This allows us to effectively extend the assimilation time T to $(b + 1)T$, but without the non-convexity issue that would occur if it would be extended directly (this was confirmed in our simulations). Moreover, the choice (3.10) introduces a strong linkage between the successive assimilation windows, and effectively allows the smoothing distribution to rely on two sided information (both from the past and the future), versus one sided information if one would simply use a longer window of length $(b + 1)T$. In fact, this was confirmed during our simulations, and we have found that increasing T beyond a certain range did not improve the performance, while increasing b has resulted in an improvement in general up to a certain point. Based on [52], we expect the Gaussian approximation underlying the choice (3.10) to hold if the observation noise is sufficiently small, the observation frequency is sufficiently high, and the system dynamics and the observations are not too non-linear.

The choice of the precision matrices (3.10) is also justifiable in the case of linear dynamics. When $b = \infty$, the precision matrix (3.10) is exactly equal to the precision matrix given by the Kalman filter, hence it is optimal. When b is finite, the precision matrix given by (3.10) is smaller (in positive definite order) than the optimal precision matrix given by the Kalman filter. This means that we might lose some precision, but do not introduce instability by a too large precision matrix. However, the memory and computational cost requirements of Kalman filter are $O(d^2)$ and $O(d^3)$, which can be prohibitive in high dimensions. For our method, these are $O(bd)$ and $O(bd)$, respectively, which are feasible even in very high dimensions.

We note that the incremental 4D-Var strategy ([17]) can be implemented here as follows. In the inner loops, we compute the gradient $\frac{\partial J}{\partial \mathbf{x}(t_0)}$ using the the adjoint equations with lower resolution models (see (3.2)). The Hessian-matrix products required to compute the $\mathbf{B}_0^{-1}[\mathbf{x}(t_0) - \mathbf{x}^b(t_0)]$ term in the gradient from the flow-dependent matrix covariances can also be computed using lower resolution models. For the Hessian matrix products in the iterative Krylov subspace solvers, we can always use the lower resolution model.

In contrast with this, in the outer loops, when computing the gradient $\frac{\partial J}{\partial \mathbf{x}(t_0)}$ we always need to use the highest resolution model (including in the Hessian-matrix products required

to compute the $\mathbf{B}_0^{-1}[\mathbf{x}(t_0) - \mathbf{x}^b(t_0)]$ term in the gradient). The Hessian-matrix products for the iterative solvers can still be computed on lower resolution models.

4 Simulations

In this section, we are going to illustrate the performance of our proposed method through simulation results. As a comparison, we also apply the ENKF and En4DVar methods on the same datasets as these form the basis of most currently used data-assimilation systems (see [15]). Section 5 of [33], [23] and Sections 7-8 of [56] offer excellent introductions to standard data assimilation methods such as 4D-Var and ENKF and its variants. Note that the literature in data assimilation is large, and many variants of 4D-Var, ENKF and hybrid methods have been proposed (see [65], [3] and [31]).

We consider three linear observation scenarios. In every scenario it is assumed that the observations happen in every h time units, and that the linear observation operators H_i are the same each time, represented by a matrix $\mathbf{H} \in \mathbb{R}^{n^o \times n}$. The scenarios are as follows.

1. We observe the velocities u and v at every gridpoint $1 \leq i, j \leq d$. All of the observation errors are i.i.d. $N(0, \sigma^2)$ random variables (i.e. $\mathbf{R}_l = \mathbf{R} = \sigma^2 \mathbf{I}_{n^o}$ for every $l \geq 0$).
2. We observe the height h at every gridpoint $1 \leq i, j \leq d$, and the velocities u and v at selected locations with spatial frequency r in both directions for a positive integer r . All of the observation errors are i.i.d. $N(0, \sigma^2)$ random variables.
3. We observe the height h at selected locations with spatial frequency r in both directions for a positive integer r . All of the observation errors are i.i.d. $N(0, \sigma^2)$ random variables.

First, we compare the performance of various methods using synthetic data. The shallow water equations were solved on the torus $[0, L]^2$ with $L = 210\text{km}$. The initial condition $\mathbf{U}(0) := (u(0), v(0), h(0))$, ocean depth H and other ODE parameters were chosen as follows,

$$\begin{aligned}
 u(0) &= 0.5 + 0.5 \sin\left(\frac{2\pi(x+y)}{L}\right), & v(0) &= 0.5 - 0.5 \cos\left(\frac{2\pi(x-y)}{L}\right), & h(0) &= 2 \sin\left(\frac{2\pi x}{L}\right) \cos\left(\frac{2\pi y}{L}\right); \\
 H &= 100 + 100(1 + 0.5 \sin\left(\frac{2\pi x}{L}\right))(1 + 0.5 \sin\left(\frac{2\pi y}{L}\right)); \\
 \nu &= 10^{-3}, & c_b &= 10^{-5}, & g &= 9.81, & f &= 10^{-4}.
 \end{aligned}$$

The discretised versions of the initial condition and the ocean depth were obtained under the choices $d = 21$, $\Delta = 10\text{km}$. In the second observation scenario we have chosen the

spatial frequency of the velocity observations as $r = 3$ (giving 49 velocity observations). Observations are made every 10 seconds, and the observation errors are i.i.d. $N(0, \sigma^2)$ random variables for $\sigma = 10^{-2}$. The background (prior) covariance matrix \mathbf{B}_0 was chosen as a diagonal matrix. The assimilation window T was chosen as 3 hours, which offered the best performance for fixed background covariance. Fig. 1 illustrates the performance of the various methods in the two observation scenarios. For the ENKF, we have used localisation, as described in Section 8.3 of [56]. The filter function in the localisation was done according to equation (8.29) of [56], and the localisation radius was tuned for optimal performance. We have also used multiplicative ensemble inflation, as described in Section 8.2 of [56], which was also tuned for optimal performance. The 4D-Var method was optimised based on the Gauss-Newton method with preconditioned conjugate gradient (PCG) based linear solver. We did not use any preconditioner, and the maximum number of iterations per PCG step was set to 100 (which was sufficient for reducing the relative residual below 0.01 in most cases). In the En4D-Var method, we used a hybrid version of the ENKF based on fixed covariances (i.e. a linear combination of them), and the optimization was done in a similar way as for the 4D-Var method. All of the methods were implemented in Matlab and ran on a single node of the Oxford ARC Arcus-B HPC cluster (16 cores per node). The measure of performance is the relative error of the unobserved component at a certain time t , i.e. if $\mathbf{w}(t) \in \mathbb{R}^{n-n^\circ}$ denotes the true value of the unobserved component, and $\hat{\mathbf{w}}(t) \in \mathbb{R}^{n-n^\circ}$ is the estimator, then $\|\hat{\mathbf{w}}(t) - \mathbf{w}(t)\|/\|\mathbf{w}(t)\|$ is the relative error ($\|\cdot\|$ refers to the Euclidean norm in \mathbb{R}^{n-n°).

We have also repeated the experiment in the most challenging third observation scenario, where we had height observations with spatial frequency $r = 3$ (giving 49 observations in total). Observations were only taken every 60 seconds (versus 10 seconds in the previous experiment), and the total observation length was 10 days (versus 1 days). The other parameters were kept the same ($d = 21$, $\Delta = 10\text{km}$, $\sigma = 10^{-2}$).

Fig. 2a shows the performance of 4D-Var with a fixed background covariance matrix with varying window sizes $T = 3\text{h}$, 6h , 9h , 12h and 18h . In the case of 12h and 18h , we have used the idea of [54] to first find the optimum for shorter windows, and then gradually extend the window length to T to avoid issues with non-convexity. This has resulted in better optimum at the cost of longer computational time (it did not make a difference at shorter window lengths). Overall, we can see that the $T = 12\text{h}$ has the best performance, but the computational time is longer than for $T = 9\text{h}$ (as we in fact first find the optimum

based on the first half of the observations in the window, and then continue with the other half). At $T = 18h$ the performance diminishes due to the non-convexity of the likelihood, and even the gradual extension of the window length fails to overcome this problem.

Fig. 2b compares the performance of our method (based on $T = 9h$, but with choices of b from 1 to 5) with 4D-Var with fixed window length ($T = 12h$), ENKF and EN4D-Var. For this synthetic dataset, our 4D-Var-based method with $b = 3$ offered the best performance. $b = 4$ was similar but with higher computational cost, and $b = 5$ resulted in worse performance, likely due to the non-linearity of the system. We can see that using observations in earlier assimilation windows to update the background covariance matrix in a flow-dependent way is very beneficial, with relative errors reduced by as much as 70-90% compared to using a fixed background matrix.

To better understand the reason for this improvement in performance, on Fig. 3 we have plotted the average correlations in background covariances between the components at a given distance, in the cases $b = 1, 2, 3$, for the first observation scenario computed at the last observation window (after 24 hours). As we can see, as b increases, the background covariance matrix changes and becomes less-and-less localised.

The performance of the ENKF and especially the En4D-Var method were quite competitive, and lead to nearly as good results as our method. However, the computational times for these methods were longer, and they required much more tuning than our method. Note that in the second observation scenario, where we have fewer observations compared to the first one, the ENKF converged quite slowly compared to the 4D-Var based approaches unless the number of particles was increased drastically, which increased the simulation time considerably.

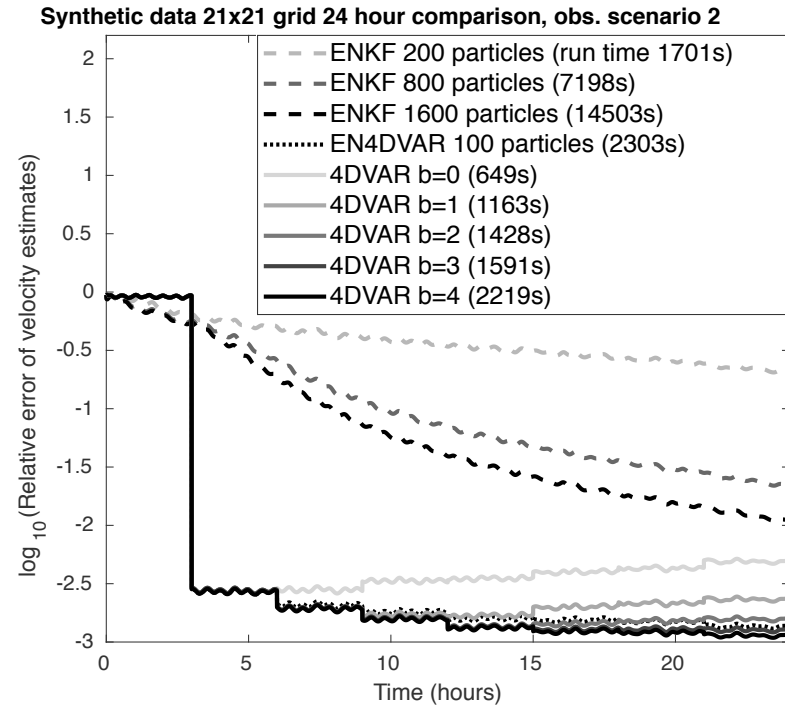
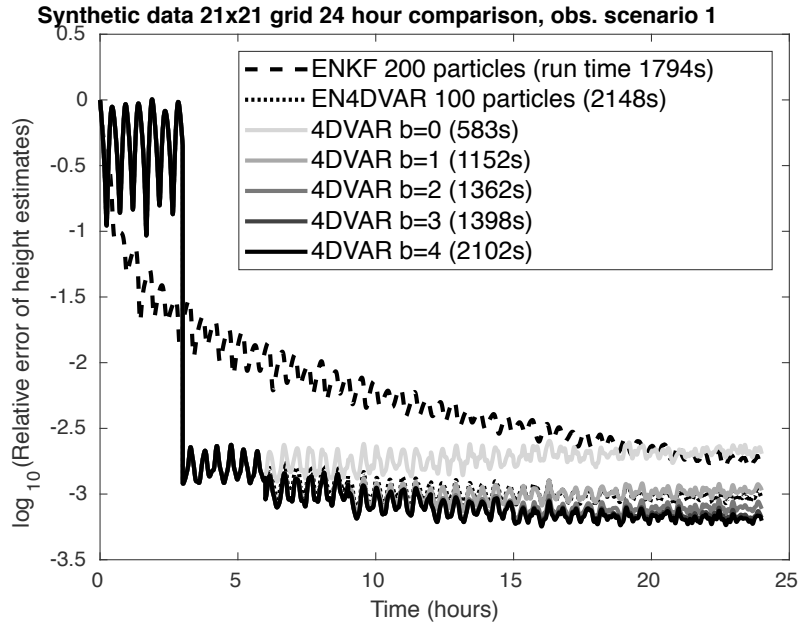
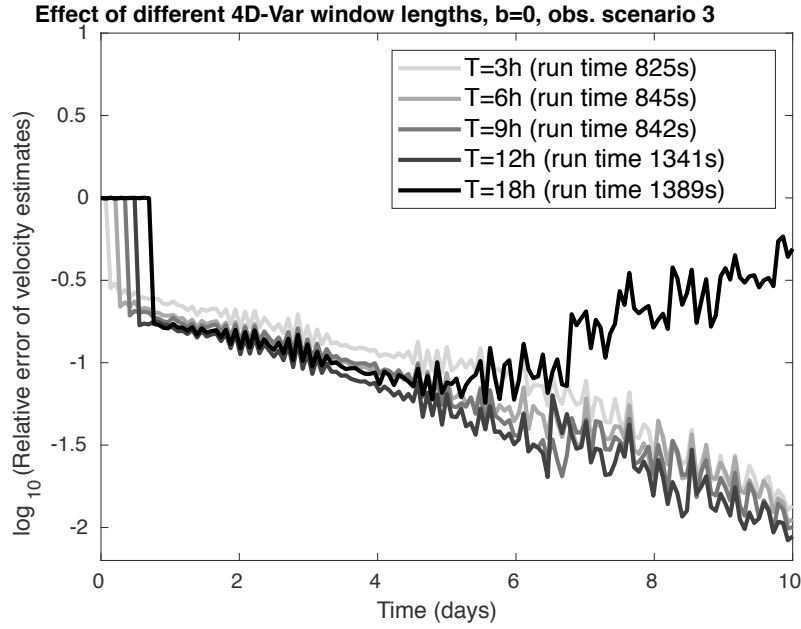
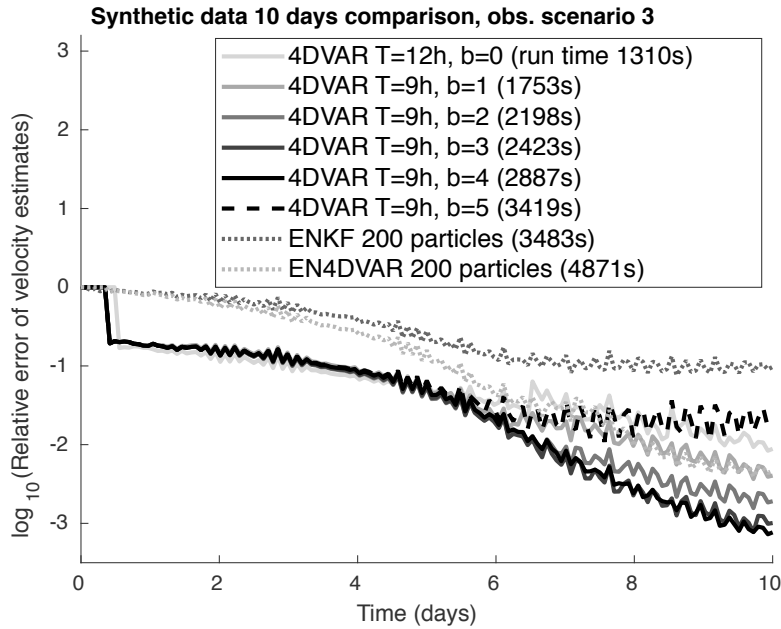


Figure 1: Relative errors of velocity estimates in the case of synthetic data for all methods. Setting: $d = 21$, $k = 1080$, $T = 3\text{h}$, $\sigma = 10^{-2}$, $\Delta = 10^4$, 10 seconds between observations. The 4D-Var and EN-4DVar methods process the data in batches of size k , hence the filtering accuracy is close to zero until we have reached the end of the first observation window.



(a)



(b)

Figure 2: Relative errors of velocity estimates for synthetic data with observation scenario 3. Setting: $d = 21$, $\sigma = 10^{-2}$, $\Delta = 10^4$, 60 seconds between observations. Fig. 2a shows the performance of 4D-Var with fixed covariance matrix for different time lengths. Fig. 2b compares the performance of our method with ENKF and En4D-Var.

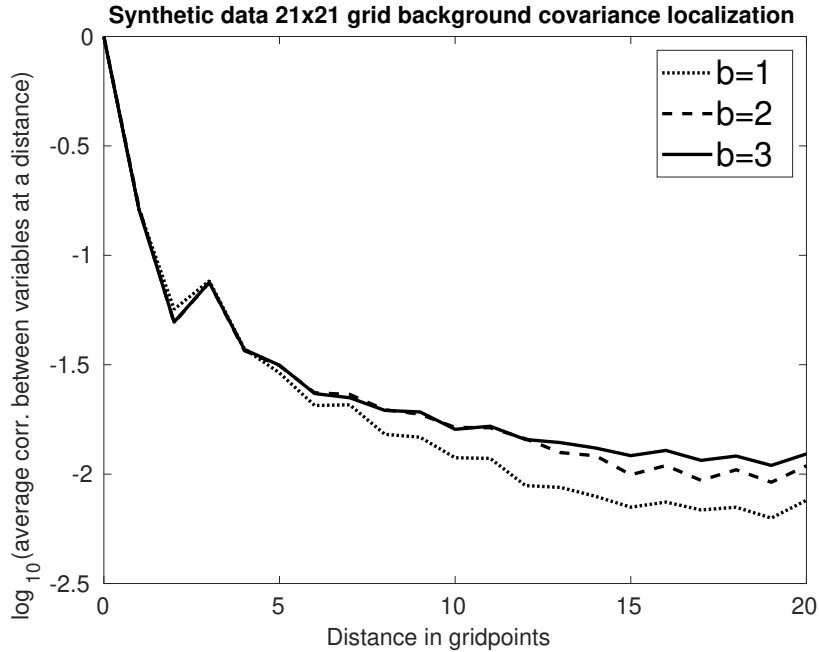


Figure 3: Correlation decay in flow-dependent background covariances for different values of b . Setting: $d = 21$, $k = 1080$, $T = 3\text{h}$, $\sigma = 10^{-2}$, $\Delta = 10^4$, observation scenario 1.

The shallow water equations are applied in tsunami modelling. [57] estimate the initial distribution of the tsunami waves after the 2011 Japan earthquake. They use data from 17 locations in the ocean, where the wave heights were observed continuously in time. We have used these estimates as our initial condition for the heights, and set the initial velocities to zero (as they are unknown). Using publicly available bathymetry data for \bar{h} , and the above described initial condition, we have run a simulation of 40 minutes for our model, see Fig. 4. We have tested the efficiency of the data assimilation methods also on this simulated dataset, considering a time interval from 10 to 40 minutes (thus the initial condition corresponds to the value of the model after 10 minutes and is shown in Fig. 4b). Due to the somewhat rough nature of the tsunami waves, in this example we have found that setting the background precision (inverse covariance) matrix \mathbf{B}_0^{-1} as zero offered the best performance for the 4D-Var and En4D-Var methods, while diagonal covariance matrices offered the best performance for the ENKF and methods (for ENKF, this matrix is only used for sampling the initial ensemble). The localised ENKF was implemented with optimally tuned ensemble inflation and localisation as described in Sections 8.2 and 8.3 of [56]. The 4D-Var method was optimised based on the Gauss-Newton method with preconditioned conjugate gradient (PCG) based linear solver without any preconditioner,

and the maximum number of iterations per PCG step was set to 500.

Fig. 5 compares the performance of the methods for this synthetic dataset implemented for grid size $d = 336$ (so the dimension on the dynamical system is $n = 3d^2 = 338,688$) in the first two observation scenarios. For the second scenario, the spatial frequency of the velocity observations was chosen as $r = 48$ (i.e. $7 \cdot 7 = 49$ velocity observations in total).

As in the previous synthetic example, the proposed 4D-Var based method offers best performance, and they require less tuning than the ENKF based methods (which are sensitive to the variance inflation and localisation parameters in this example). We believe that the relatively poor performance of the localized ENKF methods on Fig. 5b are due to the instability of the ODE in this extremely chaotic regime, and the sparsity of the velocity observations, which require very accurate covariance modelling. Note that in the case of the second observation scenario (Fig. 5b), the best performance of the En4D-Var was achieved when we have used only a fixed covariance matrix, and coefficient for the ENKF based background covariance is set to zero in the hybridization (we have tried several hundred parameter values for the inflation, localisation and hybridization). Hence in this complex situation the ENKF based background covariances did not help, while our proposed flow-dependent covariances improved the precision of the velocity estimates when using $b = 1$ and $b = 2$.

Overall, we have found that in the examples we have tried, the proposed flow-dependent background covariances performed typically 5-10% more accurately given similar computational time than well-tuned localised ENKF and En4D-Var methods. Moreover, they required very little tuning compared to the alternative methods, which were quite difficult to tune even for this relatively simple shallow-water model. We think that for more complex 3 dimensional weather models involving both spectral and spatial discretization, the difference in accuracy and tuning complexity will be even more significant. An additional advantage of the proposed method is that it only requires the user access to the adjoint and tangent linear model solvers, which are readily available in existing 4D-Var implementations. Moreover, it also adapts well to the incremental 4D-Var formulation. We believe that the improvement in performance is due to the better modelling of forecast error covariances by the 4D-Var method, which are not completely localised for this particular model when assimilating observations over longer periods.

In this section we have done a fair comparison of the proposed method with ENKF and En4D-Var based on synthetic data and perfect model assumption. We stress that this cannot

be considered as testing the accuracy and predictive performance of the data assimilation methods on “real data” (due to the fact that available real observations are very sparse and they are quite uninformative about some model parameters so comparison based on them would be very sensitive to the tuning parameters). Moreover, in real data problems, model errors can also cause significant complications. Such comparisons are beyond the scope of this paper.

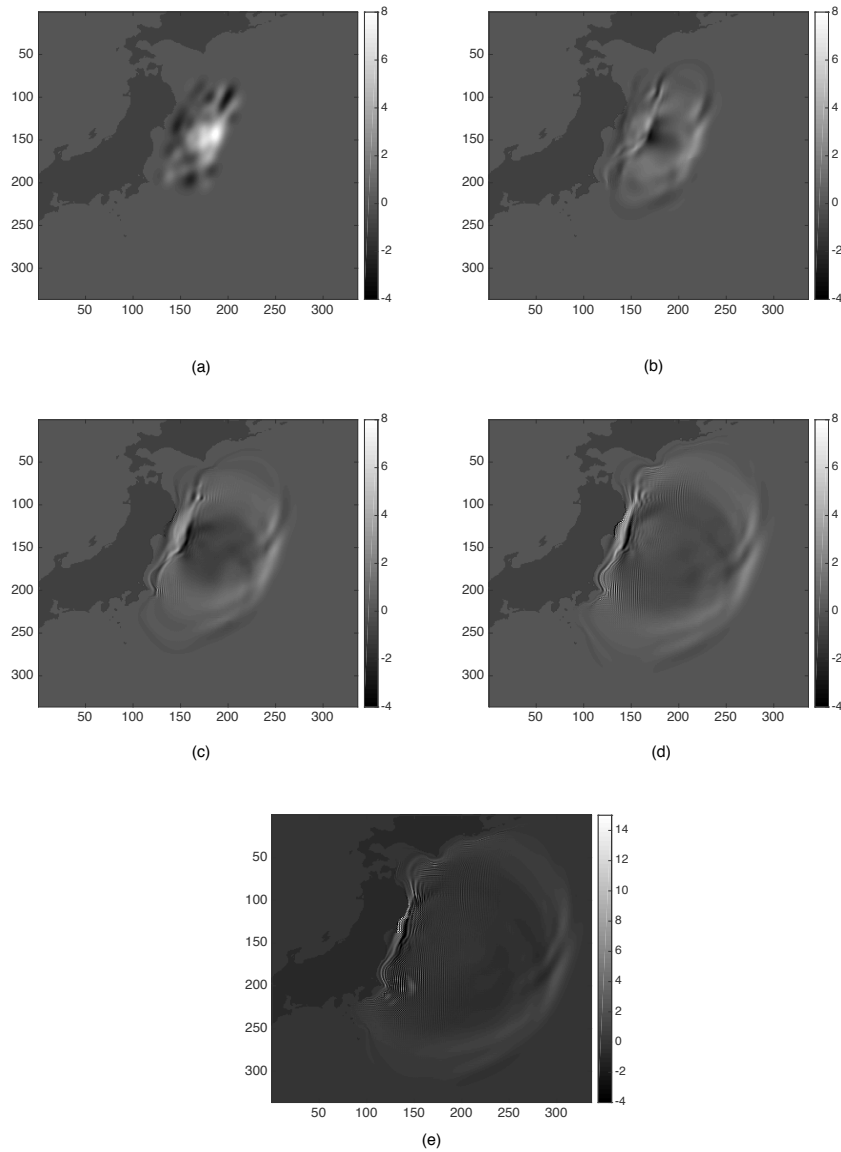


Figure 4: Evolution of the height of the tsunami waves (in meters) at 0, 10, 20, 30, and 40 mins (for grid size $d = 336$).

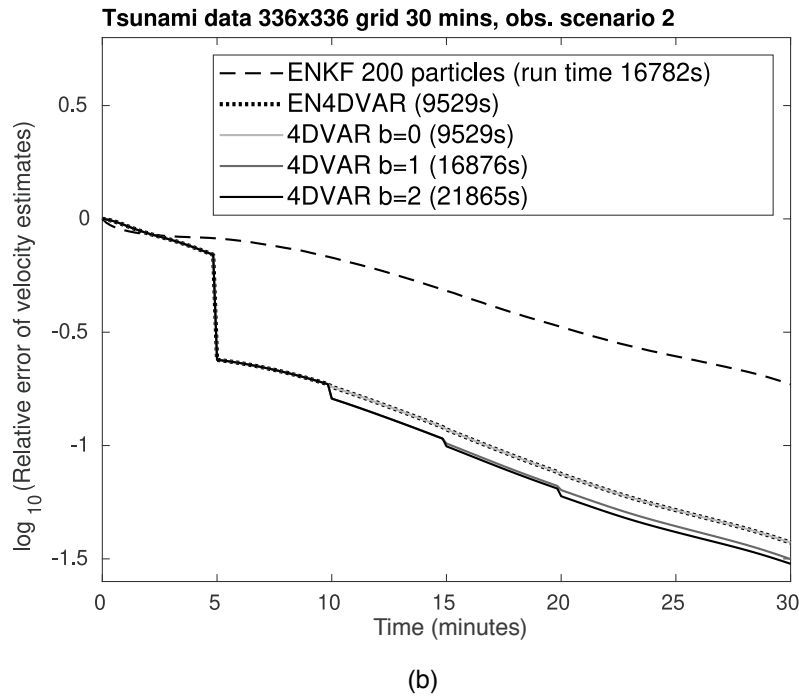
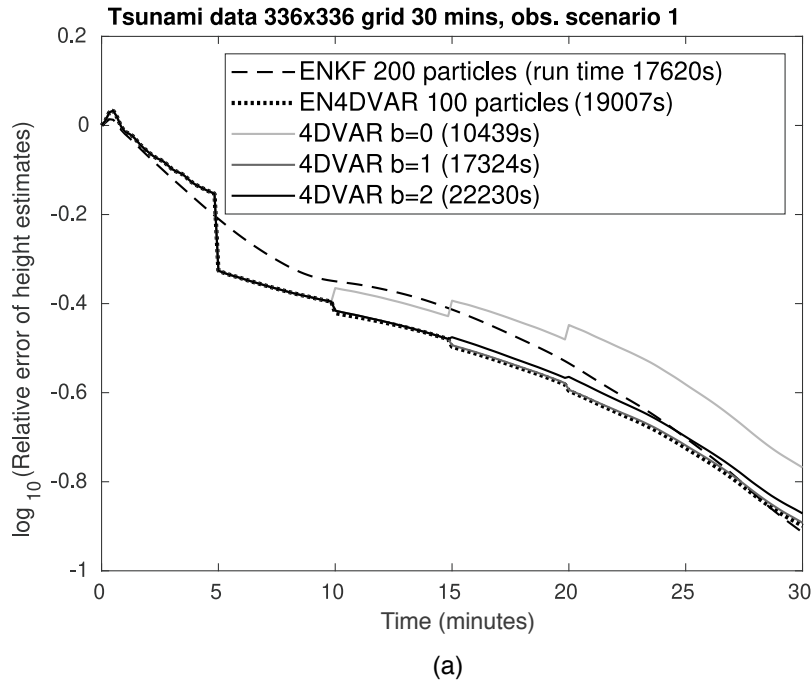


Figure 5: Relative error of estimates of velocities for tsunami data, all methods. Setting: $d = 336$, $k = 30$, $T = 30\text{mins}$, $\sigma = 10^{-2}$. In the second observation scenario, the best performance for hybrid EN4D-Var was obtained by only using the fixed background covariance matrix, hence the performance and running time is equivalent to 4D-Var with $b = 0$.

5 Conclusion

In this work we have presented a new method for updating the background covariances in 4D-Var filtering, and applied it to the shallow-water equations. Our method finds the MAP estimator of the initial position using the Gauss-Newton’s method with the Hessian matrix stored and the background covariances obtained in a factorised form. Our method is computationally efficient and has memory and computational costs that scale nearly linearly with the size of the grid. In comparisons on synthetic datasets, we have found that our method outperforms competing methods (EnKF and En4D-Var), and requires much less tuning compared to them.

Due to the definition of our method, total computational cost is at most a few times higher than 4D-Var with fixed background covariances (depending on the choice of parameter b). Since its first operational implementation in ECMWF in 1997, 4D-Var has been one of the most popular methods for numerical weather prediction and has been widely implemented. Therefore the wall-clock time and total computational cost of our method are within a practically feasible range.

4D-Var-based methods are less directly parallelisable compared to ENKF as the optimization steps and the ODE solver steps are indeed inherently serial. Nevertheless, there is large scope for parallelisation within the ODE solver due to the fact that the interactions are mostly local, and this is exploited in the operational implementations. Moreover, even if parallelisation might result in shorter wall-clock time, the energy and resource costs are proportional to the total computational time. Hence a better metric is the total computational time for a given filtering accuracy. Based on our simulations it is clear that our method is competitive in this metric with the existing ENKF and En4D-Var approaches at a given filtering accuracy.

Acknowledgements

The authors thank Joe Wallwork for providing us the tsunami data set, and for our correspondence related to the shallow-water equations. All authors were supported by an AcRF tier 2 grant: R-155-000-161-112. This material is based upon work supported in part by the U.S. Army Research Laboratory and the U.S. Army Research Office, and by the U.K. Ministry of Defence (MoD) and the U.K. Engineering and Physical Research Council (EPSRC) under grant number EP/R013616/1. AJ is affiliated with the Risk Management Institute, the Center for Quantitative Finance and the OR & Analytics cluster at NUS. DC was par-

tially supported by the EPSRC grant: EP/N023781/1. AB was supported by a Leverhulme Trust Prize. We thank Oxford Advanced Research Computing for providing us access to the HPC cluster Arcus-B for running the simulations in this paper.

A Sparse storage of Jacobians for Shallow-Water Dynamics

In this section we explain a possible method for the computation and storage of the Jacobians \mathbf{M}_i , $1 \leq i \leq k$ specifically for the case of the shallow-water equations (2.6)-(2.8). For other equations, it might be the case that storing $(\mathbf{M}_i)_{1 \leq i \leq k}$ directly as follows is not practical because the interaction between the components is not local and the Jacobian matrix is not sparse. In such cases, we can still apply the tangent-linear and adjoint equations for computing the matrix-vector products $\mathbf{M}_i v$ and $\mathbf{M}_i^T v$, as explained in Section 3.3.

One can observe that time derivatives at a grid position only depends on its grid neighbours. Moreover, the shallow-water equations are of the general form $\frac{d\mathbf{x}}{dt} = -\mathbf{A}\mathbf{x} - \mathbf{B}(\mathbf{x}, \mathbf{x}) + \mathbf{f}$, where \mathbf{A} is an $n \times n$ matrix, \mathbf{B} is a $n \times n \times n$ array, and \mathbf{f} is a constant vector in \mathbb{R}^n (note that for the shallow-water equations (2.6)-(2.8), we have $\mathbf{f} = 0$). For equations of this form, there is an efficient way of calculating the time derivatives and their Jacobians, stated in equations (3.14) and (3.16) of [52]. Based on these, one can use Taylor's expansion to compute the Jacobian $\mathbf{M}(t, s)[\mathbf{x}(s)]$, that is

$$\mathbf{M}(t, s)[\mathbf{x}(s)] \approx \mathbf{I}_n + \sum_{l=1}^{l_{\max}} \frac{\partial \left(\frac{d^l}{dt^l} \mathbf{M}(t, s)[\mathbf{x}(s)] \Big|_{t=s} \right)}{\partial \mathbf{x}(s)} \cdot \frac{(t-s)^l}{l!}, \quad (\text{A.1})$$

for some $l_{\max} > 0$. Due to the fact that the first derivatives only contain terms from neighbouring gridpoints, it is easy to see that the above approximation only has non-zero elements for gridpoints that are no more than l_{\max} steps away. This means that as long as $t - s$ is sufficiently small, the Jacobian $\mathbf{M}(t, s)[\mathbf{x}(s)]$ can be stored as a sparse matrix with $\mathcal{O}(n)$ non-zero elements. If the time interval between the observations is sufficiently small, then each of $\mathbf{M}_1, \dots, \mathbf{M}_k$ can be stored as a single sparse matrix defined by (A.1). The inverse of the Jacobian satisfies that $(\mathbf{M}(t, s)[\mathbf{x}(s)])^{-1} = \mathbf{M}(s, t)[\mathbf{x}(t)]$, so it can be calculated by (A.1) with terms $(s - t)^l$ instead of $(t - s)^l$ and $\mathbf{x}(t)$ instead of $\mathbf{x}(s)$.

At this point we note that one could attempt to use the Jacobians $\mathbf{M}(t_l, t_0)$ directly. However, for $l \ll n$, storing the Jacobians $\mathbf{M}_1, \dots, \mathbf{M}_l$ separately requires $\mathcal{O}(nl)$ memory, and the effect of $\mathbf{M}_l \mathbf{M}_{l-1} \dots \mathbf{M}_1$ on a vector can be evaluated in $\mathcal{O}(nl)$ time, while for 2D

lattices, the product $\mathbf{M}_l \cdots \mathbf{M}_1$ would require $\mathcal{O}(nl^2)$ memory, and its effect on a vector would require $\mathcal{O}(nl^2)$ time to evaluate (for 3D lattices, it would incur up to $\mathcal{O}(nl^3)$ memory and computational cost). For the same reason, for longer time intervals between observations, it is more effective to break the interval into $r > 1$ smaller blocks of equal size, and store the Jacobians corresponding to each of them. In this case, when applying the Jacobian \mathbf{M}_l on a vector, the result can be computed as the product of the Jacobians for the shorter intervals.

References

- [1] Asch, M., M. Bocquet, and M. Nodet, 2016: *Data assimilation: methods, algorithms, and applications*. SIAM.
- [2] Auligné, T., B. Ménétrier, A. C. Lorenc, and M. Buehner, 2016: Ensemble–variational integrated localized data assimilation. *Monthly Weather Review*, **144** (10), 3677–3696.
- [3] Bannister, R., 2016: A review of operational methods of variational and ensemble-variational data assimilation. *Quarterly Journal of the Royal Meteorological Society*.
- [4] Bannister, R. N., 2008: A review of forecast error covariance statistics in atmospheric variational data assimilation. i: Characteristics and measurements of forecast error covariances. *Quarterly Journal of the Royal Meteorological Society*, **134** (637), 1951–1970.
- [5] Bannister, R. N., 2008: A review of forecast error covariance statistics in atmospheric variational data assimilation. ii: Modelling the forecast error covariance statistics. *Quarterly Journal of the Royal Meteorological Society*, **134** (637), 1971–1996.
- [6] Bates, P. D., M. S. Horritt, and T. J. Fewtrell, 2010: A simple inertial formulation of the shallow water equations for efficient two-dimensional flood inundation modelling. *Journal of Hydrology*, **387** (1), 33–45.
- [7] Bengtsson, L., M. Ghil, and E. Källén, 1981: *Dynamic meteorology: data assimilation methods*, Vol. 36. Springer.
- [8] Berger, J. O., 2013: *Statistical decision theory and Bayesian analysis*. Springer Science & Business Media.

- [9] Beskos, A., D. Crisan, and A. Jasra, 2014: On the stability of sequential Monte Carlo methods in high dimensions. *Ann. Appl. Probab.*, **24**, 1396–1445.
- [10] Blayo, E., M. Bocquet, E. Cosme, and L. F. Cugliandolo, 2014: *Advanced data assimilation for geosciences*. International Summer School-Advanced Data Assimilation for Geosciences, 608 pp.
- [11] Bocquet, M., C. A. Pires, and L. Wu, 2010: Beyond Gaussian statistical modeling in geophysical data assimilation. *Monthly Weather Review*, **138** (8), 2997–3023.
- [12] Bonavita, M., E. Hólm, L. Isaksen, and M. Fisher, 2016: The evolution of the ECMWF hybrid data assimilation system. *Quarterly Journal of the Royal Meteorological Society*, **142** (694), 287–303.
- [13] Bousserez, N., D. Henze, A. Perkins, K. Bowman, M. Lee, J. Liu, F. Deng, and D. Jones, 2015: Improved analysis-error covariance matrix for high-dimensional variational inversions: application to source estimation using a 3d atmospheric transport model. *Quarterly Journal of the Royal Meteorological Society*, **141** (690), 1906–1921.
- [14] Buehner, M., 2005: Ensemble-derived stationary and flow-dependent background-error covariances: Evaluation in a quasi-operational NWP setting. *Quarterly Journal of the Royal Meteorological Society*, **131** (607), 1013–1043.
- [15] Clayton, A., A. C. Lorenc, and D. M. Barker, 2013: Operational implementation of a hybrid ensemble/4D-Var global data assimilation system at the Met Office. *Quarterly Journal of the Royal Meteorological Society*, **139** (675), 1445–1461.
- [16] Courtier, P., and O. Talagrand, 1990: Variational assimilation of meteorological observations with the direct and adjoint shallow-water equations. *Tellus A*, **42** (5), 531–549.
- [17] Courtier, P., J.-N. Thépaut, and A. Hollingsworth, 1994: A strategy for operational implementation of 4D-Var, using an incremental approach. *Quarterly Journal of the Royal Meteorological Society*, **120** (519), 1367–1387.
- [18] Crisan, D., Ed., 2017: *Mathematics Of Planet Earth: A Primer*. Advanced Textbooks In Mathematics, World Scientific Europe.
- [19] Dashti, M., and A. Stuart, 2016: The bayesian approach to inverse problems. *Handbook of Uncertainty Quantification*, 311–428.

- [20] Del Moral, P., A. Doucet, and A. Jasra, 2006: Sequential Monte Carlo samplers. *J. R. Stat. Soc. Ser. B Stat. Methodol.*, **68** (3), 411–436.
- [21] Derber, J., and F. Bouttier, 1999: A reformulation of the background error covariance in the ecmwf global data assimilation system. *Tellus A*, **51** (2), 195–221.
- [22] Egbert, G. D., A. F. Bennett, and M. G. Foreman, 1994: TOPEX/POSEIDON tides estimated using a global inverse model. *Journal of Geophysical Research: Oceans*, **99** (C12), 24 821–24 852.
- [23] Evensen, G., 2009: *Data assimilation: the ensemble Kalman filter*. Springer Science & Business Media.
- [24] Fisher, M., 2003: Background error covariance modelling. *Seminar on Recent Development in Data Assimilation for Atmosphere and Ocean*, 45–63.
- [25] Fisher, M., M. Leutbecher, and G. Kelly, 2005: On the equivalence between Kalman smoothing and weak-constraint four-dimensional variational data assimilation. *Quarterly Journal of the Royal Meteorological Society*, **131** (613), 3235–3246.
- [26] Gejadze, I. Y., G. Copeland, F.-X. Le Dimet, and V. Shutyaev, 2011: Computation of the analysis error covariance in variational data assimilation problems with nonlinear dynamics. *Journal of Computational Physics*, **230** (22), 7923–7943.
- [27] Ghil, M., S. Cohn, J. Tavantzis, K. Bube, and E. Isaacson, 1981: Applications of estimation theory to numerical weather prediction. *Dynamic meteorology: Data assimilation methods*, Springer, 139–224.
- [28] Ghil, M., and P. Malanotte-Rizzoli, 1991: Data assimilation in meteorology and oceanography. *Advances in geophysics*, **33**, 141–266.
- [29] Gratton, S., A. S. Lawless, and N. K. Nichols, 2007: Approximate Gauss–Newton methods for nonlinear least squares problems. *SIAM Journal on Optimization*, **18** (1), 106–132.
- [30] Hamill, T. M., J. S. Whitaker, D. T. Kleist, M. Fiorino, and S. G. Benjamin, 2011: Predictions of 2010’s tropical cyclones using the gfs and ensemble-based data assimilation methods. *Monthly Weather Review*, **139** (10), 3243–3247.
- [31] Houtekamer, P., and F. Zhang, 2016: Review of the ensemble Kalman filter for atmospheric data assimilation. *Monthly Weather Review*, **144** (12), 4489–4532.

- [32] Ide, K., P. Courtier, M. Ghil, and A. C. Lorenc, 1997: Unified notation for data assimilation: Operational, sequential and variational (special issue, data assimilation in meteorology and oceanography: Theory and practice). *Journal of the Meteorological Society of Japan. Ser. II*, **75 (1B)**, 181–189.
- [33] Kalnay, E., 2003: *Atmospheric Modeling, Data Assimilation and Predictability*. Cambridge University Press, Cambridge.
- [34] Kalnay, E., H. Li, T. Miyoshi, S.-C. Yang, and J. Ballabrera-Poy, 2007: 4-d-var or ensemble kalman filter? *Tellus A: Dynamic Meteorology and Oceanography*, **59 (5)**, 758–773.
- [35] Kuhl, D. D., T. E. Rosmond, C. H. Bishop, J. McLay, and N. L. Baker, 2013: Comparison of hybrid ensemble/4dvar and 4dvar within the navdas-ar data assimilation framework. *Monthly Weather Review*, **141 (8)**, 2740–2758.
- [36] Lahoz, W., B. Khattatov, and R. Menard, 2010: *Data assimilation: making sense of observations*. Springer Science & Business Media.
- [37] Law, K., A. Stuart, and K. Zygalakis, 2015: *Data assimilation*, Texts in Applied Mathematics, Vol. 62. Springer, Cham, xviii+242 pp., a mathematical introduction.
- [38] Lawless, A., S. Gratton, and N. Nichols, 2005: An investigation of incremental 4D-Var using non-tangent linear models. *Quarterly Journal of the Royal Meteorological Society*, **131 (606)**, 459–476.
- [39] Le Dimet, F.-X., I. M. Navon, and D. N. Daescu, 2002: Second-order information in data assimilation. *Monthly Weather Review*, **130 (3)**, 629–648.
- [40] Le Dimet, F.-X., and O. Talagrand, 1986: Variational algorithms for analysis and assimilation of meteorological observations: theoretical aspects. *Tellus A: Dynamic Meteorology and Oceanography*, **38 (2)**, 97–110.
- [41] Lorenc, A., 2014: Four-dimensional variational data assimilation. *Advanced Data Assimilation for Geosciences: Lecture Notes of the Les Houches School of Physics: Special Issue, June 2012*, 31.
- [42] Lorenc, A. C., 2003: Modelling of error covariances by 4D-Var data assimilation. *Quarterly Journal of the Royal Meteorological Society*, **129 (595)**, 3167–3182.

- [43] Lyard, F., F. Lefevre, T. Letellier, and O. Francis, 2006: Modelling the global ocean tides: modern insights from FES2004. *Ocean Dynamics*, **56** (5-6), 394–415.
- [44] Miller, R. N., M. Ghil, and F. Gauthiez, 1994: Advanced data assimilation in strongly nonlinear dynamical systems. *Journal of the atmospheric sciences*, **51** (8), 1037–1056.
- [45] Murray, F. J., and K. S. Miller, 2013: *Existence theorems for ordinary differential equations*. Courier Corporation.
- [46] Navon, I. M., 2009: Data assimilation for numerical weather prediction: a review. *Data assimilation for atmospheric, oceanic and hydrologic applications*, Springer, 21–65.
- [47] Park, S. K., and L. Xu, Eds., 2009: *Data assimilation for atmospheric, oceanic and hydrologic applications*, Vol. 1. Springer.
- [48] Park, S. K., and L. Xu, Eds., 2013: *Data assimilation for atmospheric, oceanic and hydrologic applications*, Vol. 2. Springer Science & Business Media.
- [49] Park, S. K., and L. Xu, Eds., 2017: *Data assimilation for atmospheric, oceanic and hydrologic applications*, Vol. 3. Springer Science & Business Media.
- [50] Parrish, D. F., and J. C. Derber, 1992: The national meteorological center’s spectral statistical-interpolation analysis system. *Monthly Weather Review*, **120** (8), 1747–1763.
- [51] Paulin, D., A. Jasra, D. Crisan, and A. Beskos, 2018: On concentration properties of partially observed chaotic systems. *Advances in Applied Probability*, **50** (2), 440–479.
- [52] Paulin, D., A. Jasra, D. Crisan, and A. Beskos, 2018: Optimization based methods for partially observed chaotic systems. *Foundations of Computational Mathematics*, doi:10.1007/s10208-018-9388-x, URL <https://doi.org/10.1007/s10208-018-9388-x>.
- [53] Pelinovsky, E., 2006: Hydrodynamics of tsunami waves. *Waves in Geophysical Fluids*, Springer, 1–48.
- [54] Pires, C., R. Vautard, and O. Talagrand, 1996: On extending the limits of variational assimilation in nonlinear chaotic systems. *Tellus A*, **48** (1), 96–121.
- [55] Rebeschini, P., R. Van Handel, and Coauthors, 2015: Can local particle filters beat the curse of dimensionality? *The Annals of Applied Probability*, **25** (5), 2809–2866.
- [56] Reich, S., and C. Cotter, 2015: *Probabilistic forecasting and Bayesian data assimilation*. Cambridge University Press, New York, x+297 pp.

- [57] Saito, T., Y. Ito, D. Inazu, and R. Hino, 2011: Tsunami source of the 2011 Tohoku-Oki earthquake, Japan: Inversion analysis based on dispersive tsunami simulations. *Geophysical Research Letters*, **38** (7).
- [58] Salmon, R., 2015: *Introduction to Ocean Waves*. Scripps Institution of Oceanography, University of California, San Diego, available at <http://pordlabs.ucsd.edu/rsalmon/111.textbook.pdf>.
- [59] Talagrand, O., 1997: Assimilation of observations, an introduction. *Journal of the Meteorological Society of Japan*, **75** (1B), 191–209.
- [60] Talagrand, O., and P. Courtier, 1987: Variational assimilation of meteorological observations with the adjoint vorticity equation. i: Theory. *Quarterly Journal of the Royal Meteorological Society*, **113** (478), 1311–1328.
- [61] Trémolet, Y., 2006: Accounting for an imperfect model in 4D-Var. *Quarterly Journal of the Royal Meteorological Society*, **132** (621), 2483–2504.
- [62] van Leeuwen, P. J., 2009: Particle filtering in geophysical systems. *Monthly Weather Review*, **137** (12), 4089–4114.
- [63] van Leeuwen, P. J., 2010: Nonlinear data assimilation in geosciences: an extremely efficient particle filter. *Quarterly Journal of the Royal Meteorological Society*, **136** (653), 1991–1999.
- [64] Wang, X., D. Parrish, D. Kleist, and J. Whitaker, 2013: Gsi 3dvar-based ensemble-variational hybrid data assimilation for ncep global forecast system: Single-resolution experiments. *Monthly Weather Review*, **141** (11), 4098–4117.
- [65] Whitaker, J. S., and T. M. Hamill, 2002: Ensemble data assimilation without perturbed observations. *Monthly Weather Review*, **130** (7), 1913–1924.
- [66] Zupanski, M., 2005: Maximum likelihood ensemble filter: Theoretical aspects. *Monthly Weather Review*, **133** (6), 1710–1726.